THE ASTROPHYSICAL JOURNAL, 512:920–928, 1999 February 20

HIGH-ENERGY SPECTRAL AND TEMPORAL CHARACTERISTICS OF GRO J1008−57

C. R. SHRADER,[1,2,3] F. K. SUTARIA,[4,5] K. P. SINGH,[4,6] AND D. J. MACOMB[1,2,7]

Received 1998 February 2; accepted 1998 September 28

ABSTRACT

A transient X-ray source, GRO J1008−57, was discovered by the Burst and Transient Source Experiment (BATSE) on board the *Compton Gamma Ray Observatory* (*CGRO*) in 1993 July. It reached a maximum intensity of about 1.4 times that of the Crab, in the 20–60 keV energy band. Pulsations in the X-ray intensity were detected at a period of 93.5 s. It has subsequently been determined to be a member of the Be star subclass of X-ray transients. In addition to BATSE, GRO J1008−57 was observed during its outburst by several pointed high-energy experiments: *ROSAT*, *ASCA*, and *CGRO*/OSSE. These nonsimultaneous but contemporaneous observations took place near and shortly after the peak of the outburst light curve. We report for the first time on a combined analysis of the *CGRO* and *ASCA* data sets. We have attempted to model the broadband high-energy continuum distribution and phase-resolved spectra. The broadband, phase-averaged continuum is well approximated by a power law with an exponential cutoff. Evidence for 6.4 keV line emission due to Fe is presented based on our spectral analysis. The energy dependence of the pulse profiles is examined in order to determine the energy at which the low-energy double-peaked profile detected by *ASCA* evolves into single-peaked pulse profile detected by BATSE. We discuss the implications of this pulse profile for the magnetic field and beam distribution for GRO J1008−57. Analysis of the BATSE and *Rossi X-Ray Timing Explorer*/ASM flux histories suggests that $P_{\rm orbital} \sim 135$ days. We further suggest that a transient disk is likely to form during episodes of outbursts.

Subject headings: binaries: close — pulsars: individual (GRO J1008−57) — stars: neutron — X-rays: stars

1. INTRODUCTION

The Burst And Transient Source Experiment (BATSE) on the *Compton Gamma Ray Observatory* (*CGRO*) detected a previously uncataloged, transient source of pulsed, 20–50 keV X-ray emission during 1993 July (Wilson et al. 1994; Bildsten et al. 1997). It was detected through temporal domain searches, which utilize Fourier transform and epoch-folding analyses, as a pulsed source with a 93.5 s period. The data used in this analysis were the Large Area Detector (LAD) 4 channel discriminator rates, which are sampled at 1.024 s intervals. The signal comes primarily from the two lowest energy channels, owing to the steep continuum shape that typically characterizes accreting neutron stars above ∼10 keV; for a detailed description of the techniques employed in BATSE studies of accretion-driven pulsars, see Bildsten et al. (1997). The source was also detected as a steady (i.e., nonpulsed) source using Earth-occultation analysis of the 16 channel, 2.048 s LAD data. For a description of the Earth-occultation method, see Harmon et al. (1992). Its pulsed flux reached a maximum of 1.4 times the Crab ($\sim 2.2 \times 10^{-9}$ ergs cm^{-2} s^{-1}, 20–50 keV) on about MJD 49,193 (1993 July 25). The best position determination forthcoming from BATSE was greater than ≥ 1.5 deg^2. Subsequent scans of the region with the Oriented Scintillation Spectrometer Experiment (OSSE) on board *CGRO* led to an improved positional error box—approximately $0.^\circ 3 \times 2.^\circ 1$—which facilitated observations with imaging X-ray instruments. The *ROSAT*/Position Sensitive Proportional Counter (PSPC) determined a position accurate to within a 15″ error radius (90% confidence; Petre & Gehrels 1994), and *ASCA* provided superior spectral information by virtue of its broader energy coverage (0.5–10 keV) with a resolution in the $(E/\Delta E) \simeq 10$–50 range; for a description of *ASCA* and its capabilities, see Tanaka, Inoue, & Holt (1994). Figure 1 depicts the outburst light curve and illustrates graphically the epochs of the OSSE and *ASCA* observations. The *ROSAT* position allowed for follow-up optical observations to attempt to identify and characterize the counterpart. Imaging in a narrowband filter centered on the hydrogen Balmer lines as well as in near-IR photometric bands by Coe et al. (1994) revealed the presence of a $V = 15.3$ mag star with excess IR emission and strong Hα emission, which are defining observational characteristics of Be stars. Their analysis suggests a highly reddened $[E(B-V) = 1.9$–$2.0]$ O9-B1 star. This level of extinction is consistent with the galactic column density derived from the X-ray data, $N_{\rm H} \simeq 0.9 \times 10^{22}$ cm^{-2}. Thus it seems highly probable that the star these authors identified is the counterpart and that GRO J1008−57 is a member of the Be star X-ray binary transient class. Because of the strong absorption toward the source combined with the soft (0.1–2.4 keV) bandpass of the PSPC, limited additional information was forthcoming from *ROSAT*. GRO J1008−57 was observed by *ASCA* about 1 month after this outburst, providing broadband (0.6–10 keV), medium-resolution X-ray observations While there was no previously cataloged X-ray source at this position, a subsequent reanalysis of an *EXOSAT*/Medium-Energy Experiment (ME) observation in 1985 centered on HD 88661 (and containing GRO J1008−57) revealed the pres-

[1] Laboratory For High-Energy Astrophysics, NASA-Goddard Space Flight Center.
[2] Universities Space Research Association, Lanham, MD.
[3] Email: shrader@grossc.gsfc.nasa.gov.
[4] Tata Institute of Fundamental Research, Mumbai, India.
[5] Email: fks@tifrvax.tifr.res.in.
[6] Email: singh@tifrvax.tifr.res.in.
[7] Email: macomb@grossc.gsfc.nasa.gov.

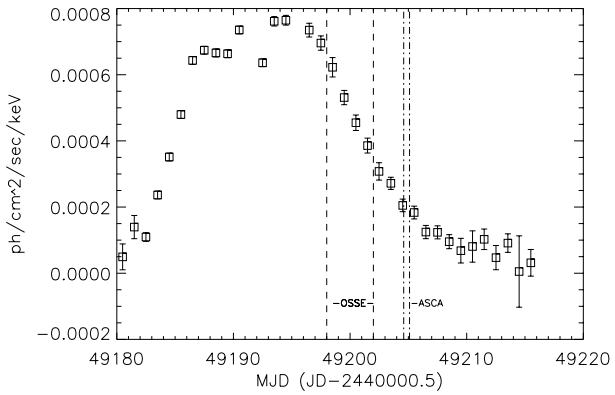

FIG. 1.—Hard X-ray (BATSE) light curve of the 1993 outburst the with *ASCA* (*dot-dashed lines*) and OSSE (*dashed lines*) observation windows indicated. The vertical axis represents the photon-flux in the pulsed component of the emission from 20–100 keV.

ence of pulsed emission at nearly the same period seen during the 1993 outburst (Macomb, Shrader, & Schultz 1994). This, combined with occasional low-level activity seen in the BATSE instruments and in the all-sky monitor experiment (ASM) on board the *Rossi X-Ray Timing Explorer* (*RXTE*) subsequent to the 1993 outburst, suggests that low-intensity transient X-ray emission—typically ~ 20 mcrab—is a characteristic of GRO J1008−57, as is much less frequent "super outburst" activity such as the 1993 event described here. In this paper we present for the first time an analysis of the combined *ASCA*, BATSE, and OSSE data sets, presenting the phase-averaged broadband X-ray energy distribution and examining the energy and possible time dependencies of the pulse profiles. The observations and data reductions are presented in § 2, spectral and temporal analyses and results based on some phenomenological and physical models are in § 3, and a discussion of the general implications for Be X-ray transients is provided in § 4.

2. OBSERVATIONS AND DATA REDUCTION

2.1. *CGRO/BATSE*

The 8 uncollimated BATSE LADs, which are located at the corners of the *CGRO* spacecraft in an octahedral arrangement, have been used extensively and with great success to monitor hard–X-ray sources using the Earth-occultation technique. For a complete description of the BATSE experiment package, see Fishman et al. (1992). The available data types for this purpose are the 16 energy-channel continuous or "CONT" data, which covers 20 keV–1.9 MeV and is sampled at 2.048 s intervals, and the LAD 4 channel discriminator or "DISCLA" data sampled every 1.024 s. Our analysis primarily utilizes the CONT data obtained subsequent to MJD 49,193. Although this data is sampled at ~ 2 s intervals, the effective time resolution in the Earth-occultation mode is essentially the ~ 90 minute orbital period of the spacecraft. The limiting 20–100 keV sensitivity of the Earth-occultation technique is typically ~ 50 mcrab (3 σ, for a 2 week observation period), depending on the level of source confusion, occultation geometry, and exposure time. For a complete description of this technique and its capabilities, see Harmon et al. (1992). For pulsed sources, additional information is available and greater sensitivity is achievable by performing a Fourier transform and epoch-folding analysis (e.g., Wilson et al. 1992; Bildsten et al. 1997). GRO J1008−57 was monitored essentially continuously with the LADs during the 1993 outburst, and both epoch-folded data and standard Earth-occultation data were obtained from the public data archive. The BATSE spectral analysis was accomplished by performing a statistically weighted summation over the 16 channel CONT data for each detector viewing the source for each *CGRO* "viewing period;" viewing periods in this context are simply the time intervals between spacecraft reorientations, used in our analysis. The resulting count spectra were then imported into the "XSPEC" analysis package (Arnaud 1996) so that a common fitting engine could be simultaneously applied to the combined, multi-instrument data sets. The response matrices used for this XSPEC data analysis were generated using software derived from the standard BATSE instrument team processing system.

2.2. *CGRO/OSSE*

GRO J1008−57 was observed with OSSE during *CGRO* viewing periods 230 and 230.5 (MJD 49,195–49,202) although the former (MJD 49,195−49,198) consisted of scanning observations performed to improve the source localization. The scanning observations have not been utilized for further analysis here. OSSE, used in standard "chopping" mode, has 440 energy channels per detector covering the 50 keV–10 MeV band with a nominal energy resolution of $E/\Delta E \simeq 12$ at 200 keV (Johnson et al. 1993; Kurfess et al. 1997). The standard ~ 2 minute on-source/off-source accumulations were analyzed using the OSSE analysis software package, IGORE, incorporating the default calibration and background model parameters. Data summation and response matrix generation were also performed using IGORE, and the resulting count spectra and response matrices were then imported into XSPEC for subsequent model fitting.

2.3. *ASCA*

GRO J1008−57 was observed by *ASCA* between MJD 49,204.6 and 49,205.1 (1993 August 5) during its postverification phase. The *ASCA* observatory is equipped with two CCD cameras, the Solid-State Imaging Spectrometers (SIS) covering 0.4–10 keV, and two Gas Imaging Spectrometers (GIS) covering 0.7–10 keV in the focal plane (Tanaka et al. 1994). The total on-source exposure time in the GIS detectors was 17.2 ks, while that on the SIS0 detector was 11.0 ks and that on SIS1 detector was 11.2 ks. The data from the SIS observations were not used in this analysis, since the source image was centered between the edges of the CCD detectors. Hence all results presented here are based on the analysis of data from the two GIS detectors (labeled GIS2 and GIS3), which have an energy resolution ($E/\Delta E$) of $\simeq 13$ at 6 keV. The data were screened by restricting the rms attitude fluctuation to within a $0\overset{\circ}{.}01$ tolerance and the minimum elevation angle with respect to the limb of the Earth to 5°. We ignored data segments obtained during passages through the South Atlantic Anomaly. The average count rate was found to be ~ 10 counts s^{-1}. Since this rate is quite high, we defined detection cells with radii $\simeq 8'$ for GIS2 and GIS3. A broadband light curve was extracted in the range of 0.7–10 keV. In addition, four light curves in the narrow energy bands of 0.6–2, 2–4, 4–6, and 6–10 keV, respectively, were also extracted. Given the intensity of GRO J1008−57 during the time of the observations, the

background was negligible and hence has been ignored. Phase-averaged and phase-resolved spectra were extracted using the standard region filters of radius $\simeq 6'$. The phase-resolved spectra were accumulated over 10 uniformly spaced phase bins, and an average background spectrum was extracted from neighboring regions surrounding the source image. The latest available version of detector response was employed in our subsequent analysis, and the default 4 channel rebinning was applied to the data. The same background spectra were used with both the phase-averaged and phase-resolved count spectra for the detailed spectral modeling.

3. DATA ANALYSIS

In the following subsections, we present the results from the timing and spectral analysis of the *ASCA* and BATSE data as well as results from the spectral analysis of the *CGRO*/OSSE data. Our timing analysis includes period determinations and pulse-profile analysis. In our spectral analysis, a variety of scenarios for modeling the continuum and evidence for line features are discussed.

3.1. *Temporal Analysis*

The *ASCA* time series data were analyzed after applying the data screening and extraction procedures described in § 2. We have neglected to apply a barycentric correction in our *ASCA* analysis based on the following arguments: The maximum barycentric displacement of the Earth/satellite system from GRO J1008−57 over our 0.5 day *ASCA* observing window is

$$\Delta t \sim (2\ \mathrm{AU})(0.5/365.25)\cos(57)/c = 0.75\ \mathrm{s}$$

or about 0.8% of a 93.5 s spin period. Since we use a 50 bin light curve for our *ASCA* analysis, the net effect is is less than half of a bin. In addition, we have used 10 bins for our phase-resolved spectroscopy, implying an error of 1/12th of a bin. A Fourier transform analysis of the broad band light curves yielded a pulse period of 93.623 ± 0.011 s from both detectors. Epoch-folded χ^2 maximization of the pulse period yielded pulse periods of 93.57 ± 0.09 s from GIS2 and GIS3 data sets. The "zero-phase" is taken as the beginning of the BATSE observation described below. Epoch folded light curves with 50 phase-bins per period were also constructed for eight energy intervals: 0.6–2, 2–4, 4–6, and 6–10 keV in the *ASCA* band (Fig. 2). The pulse profiles up to 4 keV show the clear double-peaked features that were observed by *ROSAT* (Petre & Gehrels 1994). The pulses profiles for higher energies, 20–30, 30–40, 40–50, and 50–70 keV, were constructed from the standard "ground-folded" BATSE pulsar data sets obtained from the public archives. The light curves were constructed by phase-folding data covering the interval from MJD 49,198.635–49,202.520 into 32 bins. The transition from a double-peaked profile at low-energy *ASCA* bands to a single-peaked profile seen in the high-energy bands by BATSE is continuous. In the *ASCA* 6–10 keV energy band, the pulse profile has almost evolved into the single-peaked observed by BATSE (Fig. 2). The pulse-profiles are generally smooth, lacking sharp structure. It is worth noting that a single-peaked profile was attributed to the 1–4 keV light curve in the *EXOSAT* data obtained in 1985 (Macomb et al. 1994).This suggests a luminosity dependence of the pulse-profile, perhaps with a pencil-beam geometry at low luminosities and a fan-beam geometry at higher luminosity.

3.2. *Spectral Analysis*

3.2.1. *Phase-averaged ASCA Spectra*

Spectral analysis of the *ASCA* data was carried out for both the phase-integrated and the phase-resolved data. In

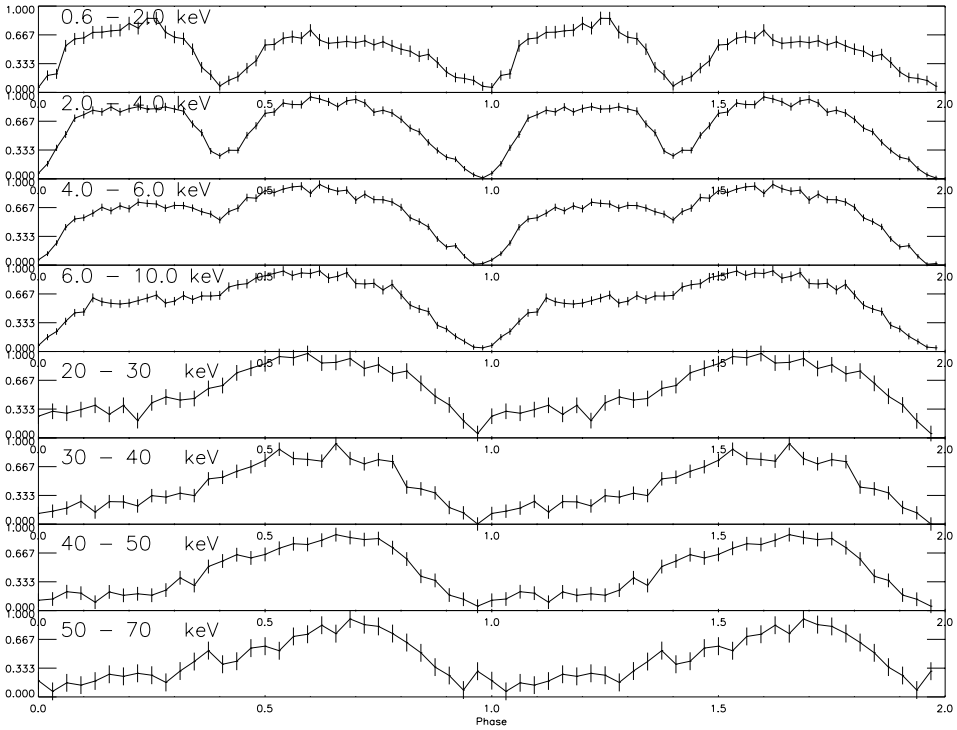

FIG. 2.—Normalized pulse profiles for GRO J1008−57 as function of energy, derived from the *ASCA* (GIS2) and BATSE data. The smooth transition from a double- to single-peaked profile with increasing energy is evident. The general lack of sharp structure is suggestive of wind rather than disk accretion.

this analysis, the data for GIS2 and GIS3 were fitted jointly, and only the normalizations were allowed to vary independently. First we discuss the spectral modeling of the phase integrated data. The following models were used for the emission component of the continuum spectra:

1. The simple power-law dependence, which has the functional dependence on energy E as $A(E/1\ \mathrm{keV})^{-\Gamma}$, where Γ is the photon index and A is a normalization factor.

2. A cutoff–power-law model, which has the energy dependence $A(E/1\ \mathrm{keV})^{-\Gamma}\exp(-E/E_{\mathrm{cutoff}})$, where E_{cutoff} is the high-energy cutoff and A and Γ are same as in (1).

3. A power law combined with a blackbody component, where the blackbody component is given by $8.0525K_{\mathrm{norm}}E^2\,dE/(kT_b)^4(\exp(E/kT_b)-1)$ and kT_b is the energy in keV. The normalization factor $K_{\mathrm{norm}} = L_{\mathrm{source}}\times 10^{-37}/D^2$, where L_{source} is the source luminosity in ergs s^{-1} and D is the source distance in kpc.

4. The "multicolor" (disk) blackbody model of Mitsuda et al. (1984), which models a spectrum from an accretion disk wherein, since the temperature is a function of the radial coordinate, multiple blackbody components are incorporated into the model. The model parameters are the temperature at the inner radius of the disk T_{in} and a factor $K = [(R_{\mathrm{in}}/\mathrm{km})/(D/10\ \mathrm{kpc})]^2\cos\theta$, where R_{in} is the inner radius of the disk and θ the inclination.

5. A simple power law with a disk-blackbody component.

6. The self-Comptonization model of Lamb & Sanford (1979), which is a function of the electron temperature kT_e, the optical depth τ, and a normalization factor. The model accounts for the Compton scattering of photons emitted by thermal bremsstrahlung.

In each case, the multiplicative absorption component was modeled using a photoelectric absorption law of the form $\exp[-N_{\mathrm{H}}\sigma(E)]$, where N_{H} is the column density and $\sigma(E)$ is the absorption photoelectric cross-section based on the tabulations of Morrison & McCammon (1983). A tabulation of various model parameters is presented in Table 1. Here we discuss individual characteristics of each model. The simple power-law model did not lead to a satisfactory fit, and thus more complex models have to be considered. Based on the continuum-only fits to the phase-averaged spectra, the column density in the direction of the source lies in the range $\sim(0.8\text{–}1.2)\times 10^{22}\ \mathrm{cm}^{-2}$. The cutoff–power-law model improved the fit considerably, while modeling the continuum with a power-law plus a blackbody component led to only a marginal improvement. A "multicolor" blackbody, which is used to model emission from a (transient) accretion disk surrounding the pulsar, does not fit as well as either (2) or (3). The self-Comptonization model (6) worked about as well as the cutoff–power-law model. In order to search for the presence of line features, an additional Gaussian component was added to the cutoff–power-law model (Fig. 3*a*). We found that the addition of a line feature at 6.57 keV corresponding to the Fe line improved the fit, as indicated by the value of the F_χ statistic, defined as $\Delta\chi^2/\chi_\nu^2$, being 38.4. The column density and photon spectral index remained nearly unchanged. The equivalent widths of the line features thus inferred are 33 and 60 eV from GIS2 and GIS3, respectively. Adding a Gaussian component to the power-law plus blackbody continuum model also improves the fit, giving $F_\chi = 37.2$; adding a Gaussian to the self-Comptonization model improves that fit considerably ($F_\chi = 21.23$) as well, leaving the optical depth and electron temperature almost unchanged. These cases thus further support the existence of the line feature (Fig. 3*c*).

3.2.2. *Phase-averaged Broadband Spectra*

We have attempted to fit the broadband phase-averaged spectra using the *ASCA* GIS combined with BATSE and/or OSSE. The midpoints of the OSSE and *ASCA* observing periods were separated by 4 days, during which time the source intensity was halved and the high-energy spectral-energy distribution was softening (based on fits to the OSSE

TABLE 1

RESULTS FROM THE ANALYSIS OF AVERAGE SPECTRA

Quantity	Cutoff Power Law (*ASCA*)	Broadband Cutoff Power Law (*ASCA*+ BATSE)	Cutoff Power Law+Gaussian (*ASCA*)	Disk-Blackbody +Gaussian (*ASCA*)	Power Law+ Disk-Blackbody Gaussian (*ASCA*)	Self-Comptonization+ Gaussian (*ASCA*)	Thermal-Bremsstrahlung with Cyclotron (OSSE+ BATSE)
N_{H} (10^{22} cm^{-2}).....	0.87 ± 0.04	0.86 ± 0.03	0.89 ± 0.04	1.14 ± 0.03	1.73 ± 0.14	1.21 ± 0.03	...
Γ	0.11 ± 0.06	0.05 ± 0.04	0.13 ± 0.07	...	5.06 ± 0.20	...	...
E_{cutoff} (keV)	5.74 ± 0.38	5.3 ± 0.2	5.78 ± 0.46	...	...	...	...
A[a]	3.79 ± 0.15	3.75 ± 0.11	3.88 ± 0.16	...	16.7 ± 5.8	2.87 ± 0.09	8.02 ± 1.68
T_{in} [b] (keV).....	...	...	...	5.43 ± 0.14	4.80 ± 0.13	...	32.7 ± 4.7
K [c]	...	...	...	0.100 ± 0.007	0.15 ± 0.01	...	...
kT_e	...	...	...	...	...	2.76 ± 0.06	...
τ	...	...	...	...	...	24.3 ± 0.6	...
E_{line} [e] (keV)	...	...	6.57 ± 0.07	6.57 ± 0.07	6.58 ± 0.07	6.61 ± 0.07	44.7
EW (eV).....	...	...	32.7	52.1	45.4	25.3	...
χ^2/degrees of freedom (d.o.f.).....	479.9/369	409/235	429.9/ 366	538/367	429.2/364	452.1/366	59/69
Flux[d]	7.46	14.3	7.44	7.51	7.45	7.39	...

[a] Unabsorbed flux at 1 keV (observer frame) in units of 10^{-2} photons cm^{-2} s^{-1} keV^{-1}.
[b] Temperature of the inner edge of the transient accretion disk.
[c] $K = (R_{\mathrm{in}})^2\cos\theta/D_{10}^2$ where R_{in} is the radius of the inner edge of the accretion disk in km, D_{10} is the distance to the source*i* and θ is the angle of the disk.
[d] In units of 10^{-10} ergs cm^{-2} s^{-1} in 2 to 10 keV energy band except *ASCA*/BATSE which is 2 to 100.
[e] Energy of the Iron line, except OSSE/BATSE which is the cyclotron energy.

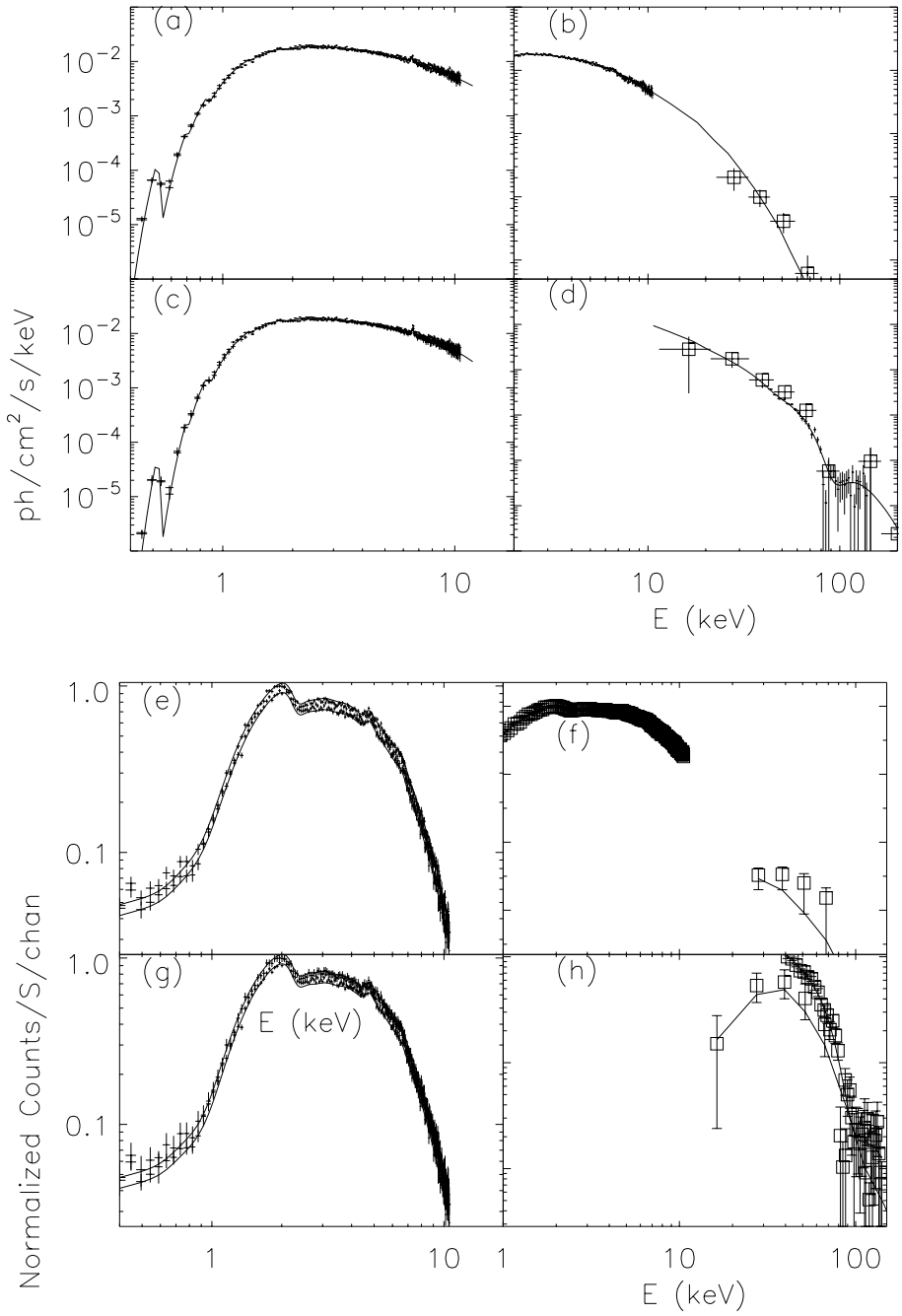

FIG. 3.—Phase-averaged spectra: (*a*) Deconvolved *ASCA* GIS spectrum. The model fitted in this case is the cutoff power law plus a Gaussian line component, as described in the text and in Table 1. (*b*) Broadband spectrum utilizing the *ASCA* GIS plus spectra derived from the BATSE LAD Earth-occultation summations. The model is a cutoff power law. (*c*) *ASCA* GIS spectral deconvolution, using the Comptonization model described in the text and summarized in Table 1. (*d*) Combined OSSE plus BATSE spectral deconvolution. A cyclotron absorption feature was included, as described in the text. (*e–h*) Corresponding count-space spectra.

and BATSE data). The OSSE spectrum was successfully fitted with a thermal bremsstrahlung model, with characteristic temperature $kT = 19$ keV. This is consistent with the results of Grove et al. (1995), but it is inconsistent with any reasonable extrapolation of the lower energy results, such as the *ASCA* power law with an exponential cutoff factor. We found (as did Grove et al. 1995) that the quality of fit is slightly improved when an absorption feature defined as in, e.g., Makishima et al. (1990) is included, the best fit centroid of the putative feature being at $E = 88$ keV. We emphasize, however, that this is a marginal result. An F-test based on our results suggests that the fit is improved at about a 2.2 σ level of confidence. Furthermore, a substantially larger value for the thermal bremsstrahlung temperature was obtained than in the case of the pure bremsstrahlung model, $kT = 32$ keV as opposed to $kT = 19$ keV, and we obtained an optical depth of $\tau = 2.2 \pm 0.6$ (Fig. 3*d*). The required magnetic field strength for a fundamental resonance at 88 keV is $B = 7.6 \times 10^{12}(1 + z)$ G, thus $\sim 10^{13}$ G assuming a gravitational redshift of $z \simeq 0.3$. Since this is at the high end of the known distribution of neutron star magnetic field strengths, it is likely that the 88 keV feature, if it is real, represents the second harmonic. The fundamental cyclotron frequency would then be at about $E_0 \simeq 44$ keV, which is

TABLE 2

RESULTS FROM SPECTRAL ANALYSIS OF GIS2 AND GIS3

Phase Interval	N_H [a]	Γ	E_{cutoff} [b]	A [c]	χ^2/d.o.f.	Flux [d]
0.0–0.1	0.97 ± 0.13	0.56 ± 0.22	7.0 ± 2.5	0.042 ± 0.006	402.8/370	4.59
0.1–0.2	0.89 ± 0.11	0.09 ± 0.18	4.2 ± 0.7	0.053 ± 0.006	480.2/370	7.49
0.2–0.3	0.82 ± -0.10	-0.03 ± 0.17	4.0 ± 0.6	0.050 ± 0.006	398.7/370	7.98
0.3–0.4	0.85 ± 0.12	-0.11 ± 0.19	4.5 ± 0.8	0.036 ± 0.005	503.7/370	7.71
0.4–0.5	0.35 ± 0.11	-0.91 ± 0.18	3.5 ± 0.5	0.013 ± 0.002	449.9/370	8.07
0.5–0.6	0.92 ± 0.11	-0.07 ± 0.17	5.1 ± 0.9	0.042 ± 0.005	411.0/370	9.92
0.6–0.7	0.82 ± 0.11	-0.28 ± 0.17	4.1 ± 0.6	0.039 ± 0.005	422.3/370	9.94
0.7–0.8	1.03 ± 0.12	0.10 ± 0.18	5.5 ± 1.1	0.048 ± 0.006	458.6/370	9.03
0.8–0.9	0.94 ± 0.12	0.28 ± 0.20	6.5 ± 1.8	0.040 ± 0.005	397.8/370	6.66
0.9–1.0	0.76 ± 0.073	0.50 ± 0.05	6.5 [e]	0.028 ± 0.002	406.1/370	3.63

NOTE.—Data is taken for different phase intervals, modeled using a cutoff power law with photoelectric absorption.

[a] In units of 10^{22} cm^{-2}.

[b] Cutoff energy in keV. The spectra is modeled as $A(E/1 \text{ keV})^{-\Gamma} \exp(-E/E_{cutoff})$.

[c] At 1 keV (in observer frame) in units of photons keV^{-1} cm^{-2} s^{-1}.

[d] In units of 10^{-10} ergs cm^{-2} s^{-1} in 2–10 keV energy band.

[e] Fixed at 6.5 keV.

below the useful low-energy sensitivity threshold for OSSE. This would indicate a field strength $B \simeq 5 \times 10^{12}$. In the 44 keV region covered by BATSE, however, the spectral resolution in the available detector modes is inadequate to resolve such a feature. A fit to the combined, simultaneously obtained BATSE–OSSE spectrum resulted in similar parameters for the 88 keV (E_1) feature, like in the fit to OSSE alone, but no evidence of the putative 44 keV feature. Using the BATSE data obtained during 1993 August 3–10, which nicely brackets the *ASCA* observations, we obtained

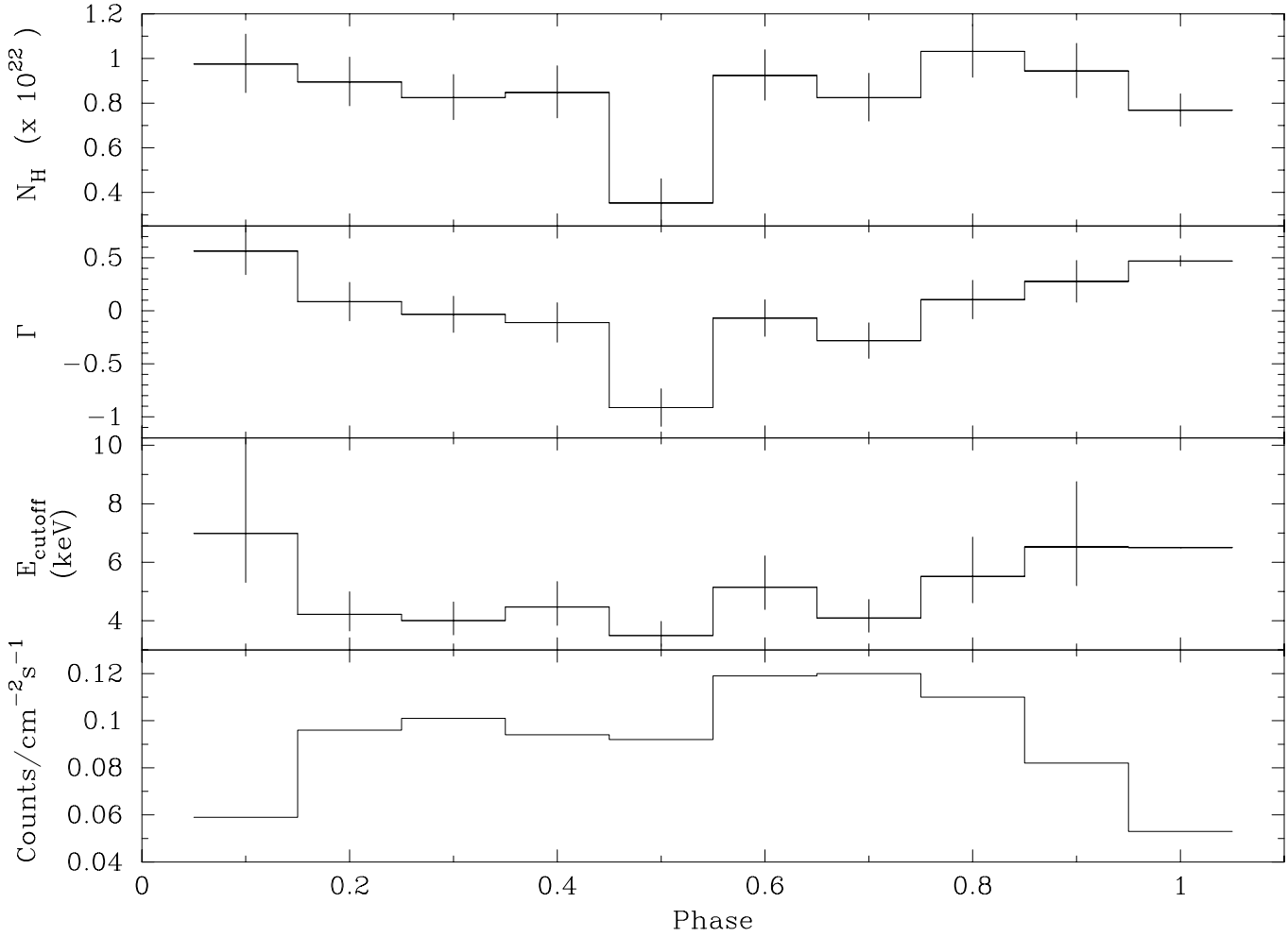

FIG. 4.—Phase-dependence of column density N_H, photon index Γ, and total flux at 0.1 phase intervals for the cutoff–power-law model. Note the sharp dip in the spectral index Γ, accompanied by a drop in the effective column density N_H at approximately phase 0.5.

a fit of an absorbed power law with a high- energy cutoff term. We were unsuccessful in fitting physical models—e.g., thermal bremsstrahlung or multiple-component models such as bremsstrahlung plus black body—to the combined data sets, nor would a single power-law fit satisfactorily. We did find, however, that we could obtain a reasonable fit for a power law, with a spectral index similar to the fits to *ASCA* alone ($\Gamma \simeq 0.8$) but including a multiplicative term equal to unity for $E < E_c$ and to $\exp(-E/E_f)$ for $E > E_c$. In this case we found, $E_c = 6$ keV and the "folding energy" $E_f = 10$ keV (Table 1; Fig. 3*b*). Ideally, one would like to be able to model the broadband continuum not just phenomenologically but with a truly self-consistent physical model. However, accretion onto strongly magnetized neutron stars is a complex problem, since it involves a full quantum treatment of the physics charged-particle dynamics in a strong magnetic field in addition to the usual uncertainties regarding details of the accretion flow. The problem of radiative breaking of particles as they accrete onto the neutron star has been treated by, e.g., Harding et al. (1984); Arons, Klein, & Lea (1987); and Miller, Wasserman, & Salpeter (1989). However, only a few attempts at computing the emergent spectrum have been made (e.g., Harding et al. 1984). We explored fitting the combined *ASCA*/GIS–*CGRO*/BATSE data to a tabulation of a grid of physical models derived from a self-consistent computation involving the accretion flow onto a magnetized neutron star; however, the resulting fits were of poorer quality than those we obtained following a phenomenological approach.

3.2.3. *Phase-resolved Spectra*

The high count rates provided by the *ASCA* detectors allowed for a detailed analysis of the phase-resolved spectra. The continuum emission models we applied for this purpose were a simple power law, a cutoff power law, a cutoff power law with a blackbody component, and a self-Comptonization model (Lamb & Sanford 1979). The GIS2 and GIS3 data were treated jointly. A simple power-law model gives χ_ν^2 in the range 1.6–1.1 and $N_{\rm H}$ in the range $(1.1–1.6) \times 10^{22}$ cm^{-2}. The cutoff–power-law model better represents the spectra with χ_ν^2 in a range from 1.4 to 1.1, while the range of variation for the parameters encompasses the values obtained from the average spectra. The phase-resolved spectra were also fitted for the self-Comptonization model, which gives χ_ν^2 in the range 1.3–1.05 for $N_{\rm H}$ in the range $(0.8–1.4) \times 10^{22}$ cm^{-2}, optical depth $\tau \simeq 11–41$, and an average electron temperature $kT_e = 2.7$ keV. Some results from this analysis are listed in Table 2. In this tabulation, a cutoff–power-law model was applied. Variations in the continuum model parameters with phase are illustrated graphically in Figure 4. The case used for illustration was the cutoff–power-law model. We note that the column density and the photon index Γ both show a dip in the phase interval 0.4–0.5, although the flux remains almost constant. Theoretical models of neutron star atmospheres assuming Coulomb-heated atmospheres and slab geometry (see Harding et al. 1984) also predict a spectral hardening toward phase intervals 0.4–0.5. It is noted that this is also the region that contains the "notch" in the pulse profile at low energies (up to 7 keV). Phase-resolved spectral analysis was also carried out for a combination of cutoff power law and a Gaussian, as well as for a simple power law plus Gaussian. These models do not fit the data well, especially since the Fe line at 6.5 keV is very weak even in the phase-integrated spectrum; thus we are unable to impose any geometric constraints on the Fe-scattering plasma.

4. DISCUSSION

Although a complete physical model of accreting neutrons star environments is lacking at present, owing to the many complexities involved, one can still in principle gain valuable basic physical insight from the properties of the phase-averaged and resolved high-energy spectra. Following Frontera & Fiume (1989; also see Harding et al. 1984), we used the broadband X-ray spectrum derived from a joint *ASCA*-BATSE spectrum fit to estimate, within the context of their model, the magnetic field strength based on the hardness ratio F_{10-20}/F_{20-100}. This hardness-ratio–based estimate of field strength B is based on the argument that, for high–magnetic-field systems having $B \sim 10^{13} G$, the hard tail of the spectrum extends to energies above 100 keV, whereas in systems with low magnetic fields (few times 10^{12}), the spectrum cuts off in the 30–40 keV range. The value for the magnetic field strength thus obtained is $\sim 6 \times 10^{12}$ G. This is similar to what one might expect for a second harmonic at 88 keV, consistent with our model fits to the OSSE spectrum, which is unfortunately inconclusive. In addition to the direct searches for an associated fundamental at 44 keV, we constructed a "Modulation Index" distribution (Frontera & Dal Fiume 1989), which is defined as $\Phi(E) = 1 - I_{\rm min}/I_{\rm max}$ (Fig. 5). Here $I_{\rm min}$ and $I_{\rm max}$ are the minimum and maximum intensities measured in a phase-folded light curve for a particular energy interval centered on E. In several other cases, including the high-mass X-ray binary (HMXB) 4U 0115+63 (Wheaton et al. 1979) and the intermediate-mass system Her X-1 (Soong et al. 1990), this modulation exhibits a discernible minimum at the cyclotron energy. Here, however, we see no evidence for a minimum in the bin containing 44 keV; rather, if structure is present at all, there is very marginal evidence for a local minimum at 25–30 keV. On the other hand, the pulse-profile is notched at low energies and smooth at high frequencies, which is characteristic of pulses that are emitted by a pencil beam from Coulomb-heated atmospheres (Harding et al. 1984). Based on this Coulomb-heated–atmosphere model of the pulsar and taking the energy at which the notch starts to vanishes as $\simeq 8$ keV, we find that the magnetic field strength is $\simeq 2.6 \times 10^{12}$ G, thus predicting a possible cyclotron resonance feature at ~ 35 keV. GRO J1008−57 was never cata-

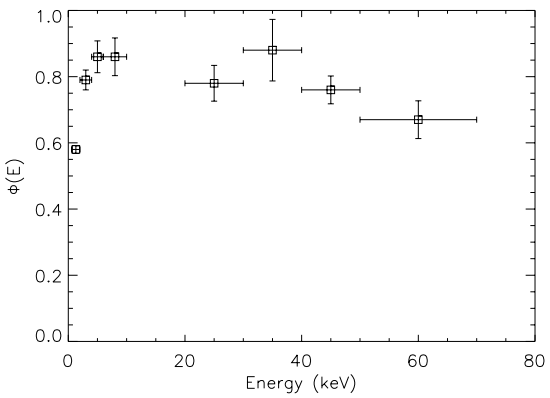

FIG. 5.—Modulation index $\Phi(E)$ as defined in the text. There is no clear indication of any structure that might be associated with cyclotron absorption, as seen, for example, in Vela X-1.

logued prior to its 1993 "discovery" with *CGRO*; however, Macomb et al. (1994) have determined that a pulsed signal was apparently present in an *EXOSAT*/ME exposure of the region obtained in 1985. In Figure 6*a*, we have graphically depicted the period history. Subsequent to the 1993 outburst, BATSE detected the source again after approximately 260 days, leading to speculation that this could be the orbital period or a multiple thereof. The time of the *EXOSAT* detection is about 30 days discrepant from an exact multiple of 260 days. Since ~11 orbits ensued between the *EXOSAT* and BATSE determinations, a difference of only 3 days would lead to such a discrepancy. It is still entirely plausible, however, that the decay tail of a more significant event was caught. In terms of the spin-orbit diagram for X-ray pulsars, the orbital period is expected to be 100 days, although there is a large amount of scatter. Recently, in 1996 April, there was evidence that the source was active once again, albeit weakly (Bildsten et al. 1997). Again, there is a moderate but tangible discrepancy with the 260 day orbital hypothesis. A review of data from the *RXTE* ASM indicates weak evidence for a possible period of about 137 days based upon a Fourier analysis of 2 yr worth of almost daily monitoring. Figure 6*b* shows the power spectrum with the peak at a frequency of 0.0003052 hr^{-1}, which is 136.5 days. This period, which is close to half the proposed period based on BATSE, will require further study before it is verified. The luminosity inferred from our determination of the 2–100 keV spectral-energy distribution at the time of the *ASCA* observations is $L_x \simeq 4.1 \times 10^{36}(d_5)^2$ ergs s^{-1}, where d_5 is the source distance in units of 5 kpc, the estimate of Coe et al. (1994). This value is about $\frac{1}{4}$ that at the outburst peak, assuming the soft X-ray flux scales in an approximately linear manner with the BATSE intensity, suggesting that the outburst luminosity was about ~10% $L_{\rm edd}$. From L_x we can estimate the mass accretion rate, $\dot{m} \sim 2.5 \times 10^{-10}\, \dot{m}\, M_\odot$ yr^{-1}. For wind accretion, assuming $\dot{m} \simeq \rho v \pi R_0^2$, where $v \sim (GM/r)^{1/2}$ and R_0 is the neutron star capture radius, the required ambient density is ~(1–2) $\times 10^{13}$ g cm^{-2}. It may be the case that the more efficient process of disk accretion is powering the X-ray source. If the magnetic field of GRO J1008−57 is $\sim 6 \times 10^{12}$ G, the Alfvén radius is $R_0 \sim 1 \times 10^9$ cm, which is ~10% of the corotation radius. Our accretion-disk model fitting, however, led to unreasonably small inner-disk radii, which certainly exclude values larger than R_0. This, combined with the generally smooth, low-amplitude pulse profiles would tend to suggest that spherical accretion from the ambient circumstellar medium was powering GRO J1008−57 at the time of our observations. On the other hand, a large change in spin-period may have occurred in this system over the period 1985–1993, for which Macomb et al. (1994) find a mean period derivative of $\langle \dot{P} \rangle \sim 7 \times 10^{-9}$ s^{-1}, and during the 1993 outburst discussed here, period derivatives $\dot{P} \simeq 3 \times 10^{-8}$ s^{-1} (both in a positive and

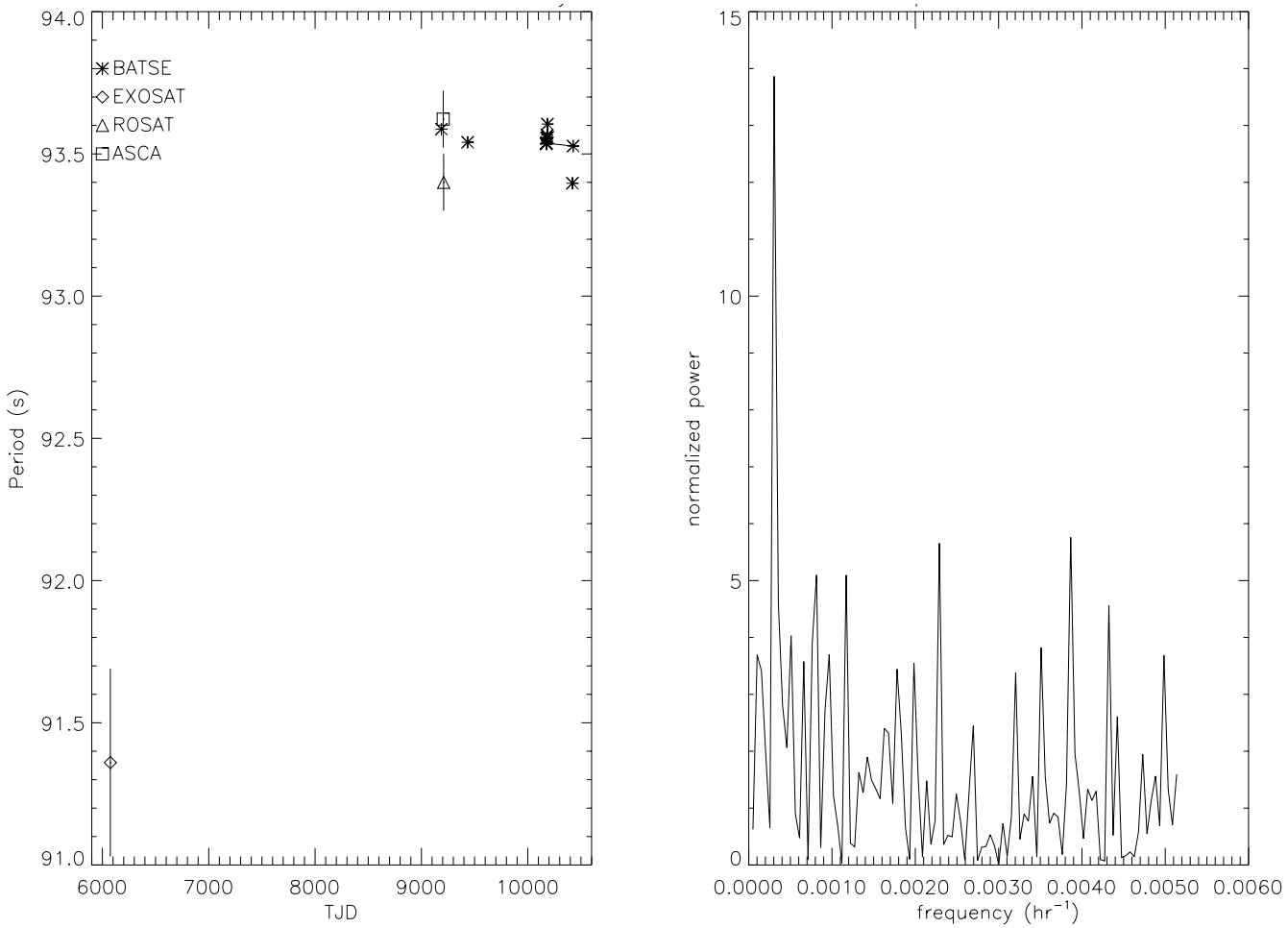

FIG. 6.—Period history based on the available *EXOSAT*, *ROSAT*, and *ASCA* data, plus the BATSE monitoring data (*left*). Fourier power-density spectrum derived from the *RXTE* ASM monitoring data (*right*). The peak at 0.0003052 hr^{-1} corresponds to a period of 136.5 days.

negative sense) are seen (Fig. 6; also see Fig. 25 of Bildsten et al. 1997). These values support a disk-accretion hypothesis; it may be the case that a transient disk forms with an inner radius which straddles the corotation radius, thus leading to intermittent periods of spin-up and spin-down. Iron emission has been seen in various accretion-driven pulsars in high-mass binaries; e.g., Vela X-1, SMC X-1, Cen X-3, and EXO 2030+375 (White, Nagase, & Parmar 1995; Makishima et al. 1986). Using our line-width determination, we can consider GRO J1008−57 in the context of the statistical distribution of Makishima (1986). It is suggested there that EW $\sim (N_{\rm H}/10^{23})$; thus a column density $N_{\rm H} \sim 0.5 \times 10^{23}$ is inferred for the ambient scattering medium. The lack of phase dependence is suggestive of an extended, spherical scattering halo; however, the statistical significance of the line detection limits our ability to constrain the geometry in any detail.

This work made use of services provided by the *Compton Gamma Ray Observatory* Science Support Center and the High-Energy Astrophysics Science Archive Research Center at the NASA Goddard Space Flight Center. The Massachusetts Institute of Technology *RXTE*/ASM online database was also utilized.

REFERENCES

Arnaud, K. A. 1996, in ASP Conf. Ser. 101, Astronomical Data Analysis Software and Systems V, ed. G. Jacoby & J. Barnes (San Francisco: ASP) 17
Arons, J., Klein, R., & Lea, S. 1987, ApJ, 312, 666
Bildsten, L., et al. 1997, ApJS, 113, 367
Coe, M. J., et al. 1994, MNRAS, 270, L57
Fishman, G. J., et al. 1992, in The Compton Observatory Science Workshop, ed. C. R. Shrader & N. Gehrels (NASA CP: 3137), 26
Frontera, F., & Dal Fiume, D. 1989, Proc. 23rd ESLAB Symp., ed. J. Hunt & B. Battrick (ESA SP-296; Paris: ESA), 57
Grove, J. E., Kurfess, J. D., Phlips, B. F., Strickman, M. S., & Ulmer, M. P. 1995, in Proc. 24th Int. Cosmic Ray Conf. (Rome: ICRC), 1
Harding, A. K., et al. 1984, ApJ, 278, 369
Harmon, B. A., et al. 1992, in The Compton Observatory Science Workshop, ed. C. R. Shrader & N. Gehrels (NASA CP: 3137), 69
Johnson, W. N., et al. 1993, ApJS, 86, 629
Kurfess, J., Bertsch, D. L., Fishman, G. J., & Schoenfelder, V. 1997, AIP Conf. Proc. 410, Fourth Compton Symposium, ed. C. D. Dermer (Woodbury, NY: AIP), 509
Lamb, P., & Sanford, P. W. 1979, MNRAS, 288, 555
Macomb, D. J., Shrader, C. R., & Schultz, A. E. 1994, ApJ, 437, 845
Makishima, K. 1986, in The Physics of Accretion onto Compact Objects, ed. K. O. Mason, M. G. Watson, & N. E. White (Berlin: Springer), 249
Makishima, K., et al. 1990, ApJ, 365, L59
Miller, G., Wasserman, I., & Salpeter, E. 1989, ApJ, 346, 405
Mitsuda, K., et al. 1984, PASJ, 36, 741
Morrison, R., & McCammon, D. 1983, ApJ, 270, 119
Petre, R., & Gehrels, N. 1994, A&A, 282, 33
Soong, Y., Gruber, D. E., Peterson, L. E., & Rothschild, R. E. 1990, ApJ, 348, 641
Tanaka Y., Inoue, H., & Holt, S. S. 1994, PASJ, 46, L37
Wheaton, W. A., et al. 1979, Nature, 282, 240
White, N. E., Nagase, F., & Parmar, A. N. 1995, in X-Ray Binaries, ed. W. H. G. Lewin, J. van Paradijs, & E. P. J. van den Heuvel (Cambridge: Cambridge Univ. Press), 1
Wilson, R. B., et al. 1992, in The Compton Observatory Science Workshop, ed. C. R. Shrader & N. Gehrels (NASA CP: 3137), 35
———. 1994, in AIP Conf. Proc. 304, Second Compton Symposium, ed. C. E. Fichtel, N. Gehrels, & J. P. Norris (New York: AIP), 390